Manipulation of dielectric particles with nondiffracting parabolic beams

Antonio Ortiz-Ambriz,[1,2] Julio C. Gutiérrez-Vega,[1,*] and Dmitri Petrov[2,3,†]

[1]*Photonics and Mathematical Optics Group, Tecnológico de Monterrey, Monterrey 64849, Mexico*
[2]*ICFO-Institut de Ciencies Fotoniques, Mediterranean Technology Park, 08860 Castelldefels (Barcelona), Spain*
[3]*Institucio Catalana de Recerca i Estudis Avancats (ICREA), Barcelona 08010, Spain*
**Corresponding author: juliocesar@itesm.mx*

Received August 4, 2014; revised October 22, 2014; accepted October 24, 2014;
posted November 4, 2014 (Doc. ID 220420); published November 20, 2014

The trapping and manipulation of microscopic particles embedded in the structure of nondiffracting parabolic beams is reported. The particles acquire orbital angular momentum and exhibit an open trajectory following the parabolic fringes of the beam. We observe an asymmetry in the terminal velocity of the particles caused by the counteracting gradient and scattering forces. © 2014 Optical Society of America

OCIS codes: (260.1960) Diffraction theory; (350.5500) Propagation; (350.4855) Optical tweezers or optical manipulation.

http://dx.doi.org/10.1364/JOSAA.31.002759

1. INTRODUCTION

The optical trapping and manipulation of small dielectric particles using optical gradient forces has attracted widespread interest since the invention of optical tweezers by A. Ashkin [1,2]. The original mechanism to transfer linear and angular momentum to particles used in optical tweezers employed basically a single light spot with an approximated Gaussian shape. It was demonstrated that particles can be stably trapped even when their diameter exceeds the trapping region of traditional Gaussian beams [3]. More recently, dynamic holography with spatial light modulators (SLMs) opened the possibility of having sophisticated shaping of light fields with exciting potential applications [4]. Perhaps the first scenario of trapping particles with structured light is the flexible creation of multiple individual spots. This situation is then equivalent to having dynamic generation of many individual traps simultaneously. Another interesting application of structured light in optical micromanipulation is the controlled and selective transfer of optical momentum to the particles. Orbital angular momentum arises in beams that have nonhomogeneous inclined wavefronts. Transfer of orbital angular momentum to microscopic particles has already been reported using Laguerre–Gauss beams [5,6], helical Bessel beams [3,7,8], and helical Mathieu beams [9,10].

In this work, we show the implementation of nondiffracting parabolic beams in optical tweezers and report the trapping and manipulation of microscopic polystyrene beads embedded in the structure of the beam. Parabolic beams constitute the fourth family of nondiffracting beam solutions to the wave equation and exhibit an unusual nonrotational phase structure across their transverse profile [11]. The experimental generation of the parabolic beam was reported some years ago [12,13], and its dynamical properties and applications in the scattering of free-falling dilute thermal atom clouds have been studied in detail as well [14–16]. The set of unitary vortices of the parabolic beam are located along the semi-axis $x > 0$, and the consequence is that particles trapped by a parabolic beam follow open parabolic trajectories. We tracked the movement of single beads to generate velocity maps that show how the particles follow the phase gradient of the parabolic beam. This work consolidates and extends previous works on trapping of dielectric particles using structured light and in particular pure nondiffracting beams [7–10].

2. DESCRIPTION OF PARABOLIC NONDIFFRACTING BEAMS

Parabolic nondiffracting beams are monochromatic solutions to the wave equation when separated in parabolic coordinates [11,12]. We first briefly describe parabolic beams in order to establish notation and to provide a reference point for necessary formulas [17]. The parabolic cylindrical coordinates (ξ, η, z) are defined by $x = (\eta^2 - \xi^2)/2$, $y = \xi\eta$, $z = z$, where $\xi \in [0, \infty)$ and $\eta \in (-\infty, \infty)$. In terms of these coordinates, the field distributions across the transverse plane $\mathbf{r}_t = (x, y)$ of the even and odd stationary parabolic nondiffracting beams $U(\mathbf{r}_t; a)\exp(\mathrm{i}k_z z)$ are given by [11,12]

$$U_e(\mathbf{r}_t; a) = \frac{|\Gamma_1|^2}{\pi\sqrt{2}} \mathrm{P}_e(\sigma\xi; a)\mathrm{P}_e(\sigma\eta; -a), \tag{1}$$

$$U_o(\mathbf{r}_t; a) = \frac{2|\Gamma_3|^2}{\pi\sqrt{2}} \mathrm{P}_o(\sigma\xi; a)\mathrm{P}_o(\sigma\eta; -a), \tag{2}$$

where $a \in (-\infty, \infty)$ is the parabolicity parameter of the beam, $\sigma \equiv (2k_t)^{1/2}$, $\Gamma_1 \equiv \Gamma(1/4 + \mathrm{i}a/2)$, $\Gamma_3 \equiv \Gamma(3/4 + \mathrm{i}a/2)$, and the transverse k_t and longitudinal k_z wave vector components satisfy the relation $k^2 = \omega^2/c^2 = k_t^2 + k_z^2$. Here, $\mathrm{P}_e(v; a)$ and $\mathrm{P}_o(v; a)$ are the even and odd real solutions of the parabolic

cylinder differential equation $(d^2/dx^2 + x^2/4 - a)P(x;a) = 0$, respectively. Theoretical patterns of stationary parabolic nondiffracting beams are shown in Ref. [11] for several values of the parameter a.

Traveling solutions can be constructed from the even and odd stationary parabolic nondiffracting beams by the linear superposition [11]

$$U^{\pm}(\mathbf{r}_t;a) = U_e(\mathbf{r}_t;a) \pm iU_o(\mathbf{r}_t;a). \tag{3}$$

In Fig. 1, we show the experimental transverse and longitudinal intensity patterns of a parabolic beam $U^{+}(\mathbf{r}_t;a)$ with parameter $a = 3$. The beam was generated with the experimental setup described in the following section. For $a > 0$, the transverse intensity pattern consists of well-defined nondiffracting parabolic fringes with a dark parabolic region around the positive x axis. The overall phase of this beam travels around the semiplane $(x \geq 0, z)$ for $a > 0$. When observed at fixed transverse planes, the phase follows confocal parabolic trajectories. The sign in Eq. (3) defines the traveling direction. By scanning the z position of the microscope objective, we are able to measure the transverse intensity distribution at different planes. This gives the (x, z) cross-section, illustrating the invariant propagation of the parabolic beam. In Fig. 1(b), the propagation invariance could be observed here over a distance of about ± 20 μm in the z direction. Similar values were found for different parabolic beams, as the length of invariance mainly depends on experimental parameters that were kept constant.

The transverse component of traveling parabolic beams with $a > 0$ has been observed to present an array of vortices along the semi-axis $x > 0$ ($x < 0$ for $a < 0$). This phenomenon suggests that parabolic beams may transfer orbital angular momentum to dielectric particles in a fashion similar to that of helical Bessel or Mathieu beams [9]. However, the structure of parabolic beams is unique in that it shows open trajectories that also transfer linear momentum. This transfer of linear momentum can be traced back to the asymmetry in the angular spectrum of parabolic beams.

3. EXPERIMENTAL ARRAY

Figure 2(a) shows the experimental array used to generate the parabolic beams and to manipulate small particles with them. We used a diode-pumped solid state laser with a wavelength of 532 nm and a measured output power of 250 mW. The beam is expanded with a telescope array composed of a divergent lens with focal length of −30 mm and a convergent lens of focal length 450 mm. The collimated beam is reflected by a (SLM, Holoeye LC-R 2500), which is addressed by a computer

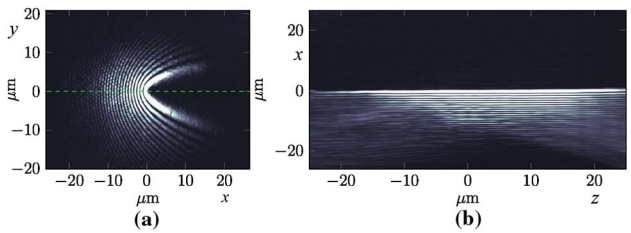

Fig. 1. Experimental transverse and longitudinal intensity patterns of a parabolic beam. The green dotted line in the first image corresponds to the cut shown in the second panel.

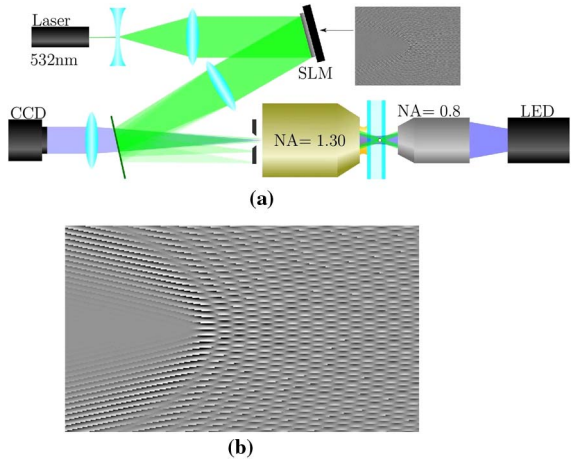

Fig. 2. (a) Experimental array used to generate parabolic beams and manipulate small particles. (b) Zoom of the central part of the hologram.

through a digital video interface. The modulated beam is then focused by a lens with a focal length of 750 mm. The focal plane of the beam is placed at the back entrance of a high-numerical-aperture (NA) microscope objective (NA = 1.30, Nikon plan fluorite oil immersion).

The beam is then focused into a custom-made fluid chamber. The chamber is made of two glass coverslips with 100 μm thickness, separated by a layer of parafilm of about 60 μm. The focal plane of the microscope objective is placed at the interface between the farthest coverslip and the fluid. On the other side of the chamber, an LED incoherent light source and a low-aperture objective (NA = 0.85) are placed to illuminate the chamber. The illumination light is then collimated to obtain a microscope image at a CCD placed at the back of the high-NA objective.

The parabolic beam was formed by modulating the phase of the beam as a blazed hologram with the SLM. In Fig. 2(b), we show the central part of the hologram. The used SLM modulates mostly the phase of the beam, but a small change in the amplitude is also present. To filter out everything that is not the angular spectrum of the parabolic beam, the axis of propagation was shifted by adding the phase of an inclined plane wave to the phase of the parabolic beam. We found that the intensity distribution of the beam is more faithfully represented if the resulting hologram is weighted by the amplitude of the parabolic beam. The expression used to calculate the hologram is then $H = |U^{\pm}(\mathbf{r}_t;a)|\{[kx\sin(\theta) + \arg(U^{\pm}(\mathbf{r}_t;a))] \bmod 2\pi\}$, where k is the wave number, x is the distance from the center of the SLM, and θ is the angle between the inclined plane wave and the optical axis. The microscope objective is shifted off the optical axis, and a diaphragm is placed before the objective to ensure that only the angular spectrum of the parabolic beam is focused into the chamber. The power of the filtered beam before entering the objective was 8 mW.

Inside the fluid chamber, we placed a low-concentration solution of 1 μm polystyrene microspheres with refractive index of 1.59 at 532 nm immersed in pure water with $n = 1.33$. We trapped a single bead with the parabolic beam. Because nondiffracting beams are nearly invariant when propagated, no trapping occurs in the propagation direction. The bead is then pushed by the radiation pressure. Setting the focal

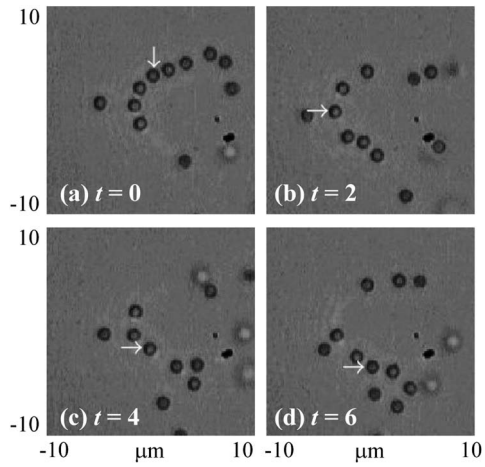

Fig. 3. Particles moved by a downward-propagating parabolic beam at 2 s intervals (see Media 1).

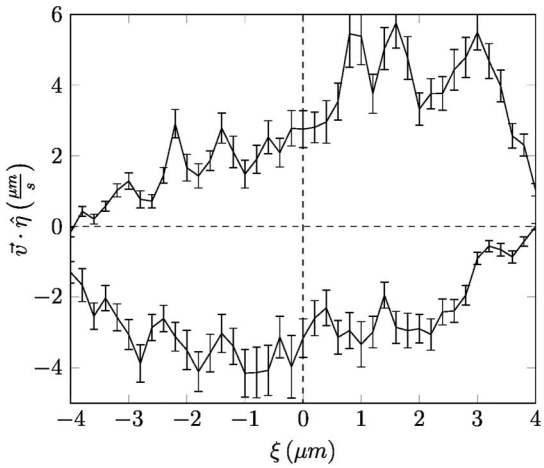

Fig. 5. Velocities of the particle in the direction of variation of the parabolic coordinate η. The upper (positive) line is the upward-traveling particle and the lower (negative) is the downward-traveling particle. It is interesting to see that the maximum velocity in both cases is not on the axis. This is because the scattering force and gradient force have different symmetry.

plane of the microscope against the second coverslip allows us to trap the bead against the glass. We can then observe the transverse effect of the beam on the microsphere.

4. PHYSICAL DISCUSSION

Figure 3 shows the motion of several beads immersed in a parabolic beam $U^+(\mathbf{r}_t; a)$ at different points in time (see Media 1). First, the particles are found to align with the parabolic fringes. It is also observed that particles drift toward the brightest fringe due to gradient force. A large Brownian component to the particle motion is present. This is mainly due to the fact that particles are only trapped in one dimension. The velocity of the displacement along a fringe is then not constant, but a stochastic movement. It is, however, evident that the average of this movement is along the direction of the phase of the traveling parabolic beam.

To avoid particle interactions, we placed a single bead in the parabolic beam and tracked its movement with standard particle-tracking algorithms [18]. The particle velocity was averaged at different points along the main fringe to create the velocity map shown in Fig. 4. Two types of beams were measured: Fig. 4(a) shows an upward traveling beam, $U^+(\mathbf{r}_t; a)$, and Fig. 4(b) shows a downward traveling beam, $U^-(\mathbf{r}_t; a)$. The switching between the two beams was done by inverting the phase of the parabolic beam in the hologram but leaving the plane wave component constant. In both these maps, it can be seen that the velocity of the particles when approaching the center of the beam is larger than the velocity when they travel away from the center. In fact, this phenomenon can be better observed in Fig. 5, where we show the component of the velocity tangential to the parabolic trajectory for upward (upper line) and downward (lower line) traveling. This phenomenon occurs because there are two forces at play in inducing the motion on the dielectric particles, the gradient force and the scattering force. The direction of the scattering force is in both cases defined by the direction of the variation of the phase. The phase increases in the direction of the unit vector $\hat{\eta}$ for $U^+(\mathbf{r}_t; a)$ and $-\hat{\eta}$ for $U^-(\mathbf{r}_t; a)$. On the other hand, the gradient force pushes the particle toward the region with higher intensity. Along a fringe of a parabolic beam, the higher intensity is toward the y axis. In fact, this is the force responsible for aligning the particles along the fringes of the parabolic beams. These two forces act on the particle in the same direction when it approaches the center of the beam, but counteract when the particle leaves the beam and thus the asymmetry of the velocity.

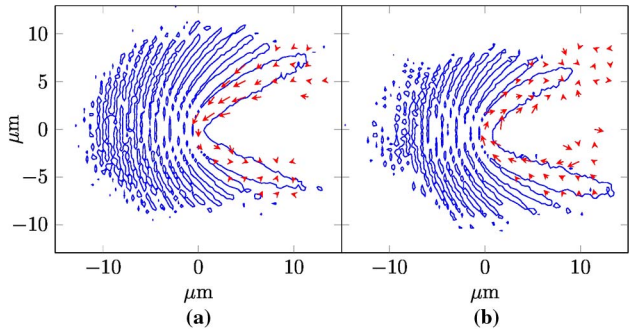

Fig. 4. Map of the directions of movement in the pattern. A grid was established and the velocity of every particle in a cell was averaged. Every point on the grid then shows an arrow which indicates the direction of the average movement. Subplot (a) shows an upward-traveling beam. Subplot (b) shows a downward-traveling beam.

5. CONCLUSIONS

We show the implementation of propagation-invariant parabolic beams in optical tweezers. We have demonstrated that dielectric microscopic particles in a parabolic beam follow parabolic trajectories. The movement along these trajectories is caused by two underlying mechanisms, namely, the scattering force in the direction of the traveling of the parabolic beam and the gradient force that pushes particles toward the center. We believe these kinds of beams to be important to complete the picture of the behavior of fundamental families of nondiffracting beams. However, we have also found the trajectories to present properties that are unique among the previously studied nondiffracting beams such as non-closed intensity fringes.

ACKNOWLEDGMENTS

We would like to thank Lluís Torner for bringing the authors together and Raúl A. Rica, Ignacio A. Martínez, and Pau

Mestres for fruitful discussion. This research was partially supported by CONACyT grant 182005, and by the Tecnológico de Monterrey Research Chair in Optics grant CAT141.

†Dmitri Petrov passed away on February 4th of 2014.

REFERENCES

1. A. Ashkin, "Acceleration and trapping of particles by radiation pressure," Phys. Rev. Lett. **24**, 156–159 (1970).
2. A. Ashkin, J. M. Dziedzic, J. E. Bjorkholm, and S. Chu, "Observation of a single beam gradient force optical trap for dielectric particles," Opt. Lett. **11**, 288–290 (1986).
3. J. Arlt, V. Garces-Chavez, W. Sibbett, and K. Dholakia, "Optical micromanipulation using a Bessel light beam," Opt. Commun. **197**, 239–245 (2001).
4. M. Wördemann, *Structured Light Fields: Applications in Optical Trapping, Manipulation, and Organisation* (Springer, 2012).
5. H. He, M. E. J. Friese, N. R. Heckenberg, and H. Rubinsztein-Dunlop, "Direct observation of transfer of angular momentum to absorptive particles from a laser beam with a phase singularity," Phys. Rev. Lett. **75**, 826–829 (1995).
6. N. B. Simpson, K. Dholakia, L. Allen, and M. J. Padgett, "Mechanical equivalence of spin and orbital angular momentum of light: an optical spanner," Opt. Lett. **22**, 52–54 (1997).
7. K. Volke-Sepulveda, V. Garces-Chavez, S. Chavez-Cerda, J. Arlt, and K. Dholakia, "Orbital angular momentum of a high-order Bessel light beam," J. Opt. B **4**, S82–S89 (2002).
8. G. Milne, K. Dholakia, D. McGloin, K. Volke-Sepulveda, and P. Zemánek, "Transverse particle dynamics in a Bessel beam," Opt. Express **15**, 13972–13987 (2007).
9. C. López-Mariscal, J. C. Gutiérrez-Vega, G. Milne, and K. Dholakia, "Orbital angular momentum transfer in helical Mathieu beams," Opt. Express **14**, 4182–4187 (2006).
10. C. Alpmann, R. Bowman, M. Woerdemann, M. Padgett, and C. Denz, "Mathieu beams as versatile light moulds for 3D micro particle assemblies," Opt. Express **18**, 26084–26091 (2010).
11. M. A. Bandres, J. C. Gutiérrez-Vega, and S. Chávez-Cerda, "Parabolic nondiffracting optical wave fields," Opt. Lett. **29**, 44–46 (2004).
12. C. López-Mariscal, M. A. Bandres, S. Chávez-Cerda, and J. C. Gutiérrez-Vega, "Observation of parabolic nondiffracting optical fields," Opt. Express **13**, 2364–2369 (2005).
13. C. López-Mariscal, M. A. Bandrés, and J. C. Gutiérrez-Vega, "Observation of the experimental propagation properties of Helmholtz-Gauss beams," Opt. Eng. **45**, 068001 (2006).
14. B. M. Rodriguez-Lara and R. Jáuregui, "Dynamical constants of structured photons with parabolic-cylindrical symmetry," Phys. Rev. A **79**, 055806 (2009).
15. B. M. Rodriguez-Lara and R. Jáuregui, "Single structured light beam as an atomic cloud splitter," Phys. Rev. A **80**, 011813 (R) (2009).
16. C. L. Hernández-Cedillo, S. Bernon, H. Hattermann, J. Fortágh, and R. Jáuregui, "Scattering of dilute thermal atom clouds on optical Weber beams," Phys. Rev. A **87**, 023404 (2013).
17. P. M. C. Morse and H. Feshbach, *Methods of Theoretical Physics*, Vol. **2** of International Series in Pure and Applied Physics (Feshbach, 1953).
18. J. C. Crocker and D. G. Grier, "Methods of digital video microscopy for coloidal studies," J. Colloid Interface Sci. **179**, 298–310 (1996).